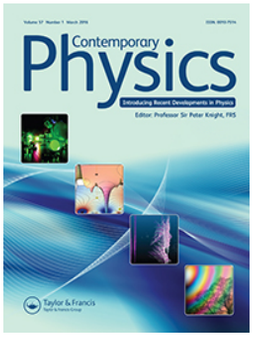

Contemporary Physics

ISSN: 0010-7514 (Print) 1366-5812 (Online) Journal homepage: http://www.tandfonline.com/loi/tcph20

Sub-cycle light transients for attosecond, X-ray, four-dimensional imaging

Hanieh Fattahi

To cite this article: Hanieh Fattahi (2016): Sub-cycle light transients for attosecond, X-ray, four-dimensional imaging, Contemporary Physics, DOI: 10.1080/00107514.2016.1231870

To link to this article: http://dx.doi.org/10.1080/00107514.2016.1231870

Published online: 03 Oct 2016.

CONTEMPORARY PHYSICS, 2016
http://dx.doi.org/10.1080/00107514.2016.1231870

Taylor & Francis
Taylor & Francis Group

Sub-cycle light transients for attosecond, X-ray, four-dimensional imaging

Hanieh Fattahi[a,b]

[a]Max-Planck Institut für Quantenoptik, Garching, Germany; [b]Department für Physik, Ludwig-Maximilians-Universität München, Garching, Germany

ABSTRACT

This paper reviews the revolutionary development of ultra-short, multi-TW laser pulse generation made possible by current laser technology. The design of the unified laser architecture discussed in this paper, based on the synthesis of ultrabroadband optical parametric chirped-pulse amplifiers, promises to provide powerful light transients with electromagnetic forces engineerable on the electron time scale. By coherent combination of multiple amplifiers operating in different wavelength ranges, pulses with wavelength spectra extending from less than 1 μm to more than 10 μm, with sub-cycle duration at unprecedented peak and average power levels can be generated. It is shown theoretically that these light transients enable the efficient generation of attosecond X-ray pulses with photon flux sufficient to image, for the first time, picometre-attosecond trajectories of electrons, by means of X-ray diffraction and record the electron dynamics by attosecond spectroscopy. The proposed system leads to a tool with sub-atomic spatio-temporal resolution for studying different processes deep inside matter.

ARTICLE HISTORY
Received 16 April 2016
Accepted 30 August 2016

KEYWORDS
Attosecond, X-ray pulse generation; waveform synthesiser; Yb:YAG thin-disc lasers; optical parametric chirped-pulse amplification; 4-D imaging

1. Does a sub-cycle pulse exist?

Years ago when I started my PhD, a senior scientist at our institute confronted me with a seemingly simple question: How short can a laser pulse be?

After a second, I replied that the pulse duration is inversely proportional to the spectral bandwidth. The larger the bandwidth, the shorter the pulse duration. However, it also depends on the central frequency of the spectrum. He seemed to be convinced. Nonetheless, there were naturally follow-up questions: Does a sub-cycle pulse exist, and can a sub-cycle pulse propagate according to Maxwell's equations? Admittedly, these were not questions that could be answered in a second!

Based on the Fourier theory, for every event in the time domain, one can define a replica in the frequency domain. These two domains are inversely proportional, meaning that a pulse with a shorter temporal duration ($\Delta\tau$) has a larger spectral bandwidth ($\Delta\omega$) (see Figure 1):

$$\Delta\tau \geq \frac{2\pi}{\Delta\omega}. \tag{1}$$

Multiple-frequency pulses or short pulses can be described by the constructive superposition of many sinusoidal waves with infinitely long temporal duration, at different carrier frequencies with the amplitude and phase given by $\tilde{E}(\omega)$:

$$E(t) = \int_{-\infty}^{\infty} \tilde{E}(\omega) e^{i\omega t} \mathrm{d}\omega. \tag{2}$$

This is the principle behind few-cycle-pulse mode-locked lasers [1]. Short pulses or even sub-cycle pulses can also be generated by superimposing several pulses at different carrier frequencies and longer temporal duration. The constructive interference region obtained from this superposition can result in waveforms with a temporal duration shorter than each individual pulse. Furthermore by fine-tuning the relative phase and amplitude between the superimposed pulses, arbitrary non-sinusoidal waveforms, called light transients, can be generated, forming the basis of temporal or spectral synthesis [2].

Light transients propagate in a medium similar to multi-cycle or few-cycle pulses as their generation is based on superposition of multi- or few-cycle pulses. Propagation of a multi-cycle pulse can be described by the slowly varying envelope approximation (SVEA), where the pulse is represented by the product of an envelope and a fast oscillating carrier wave at angular frequency of ω_0 and carrier-envelope phase of φ_{CE} [5]:

$$E(t) = f(t)\cos(\omega_0 t + \varphi_{\mathrm{CE}}). \tag{3}$$

Alternatively, the electric field can be represented as a product of a complex envelope $\mathcal{E}(t)$ and exponential of the fast oscillating wave:

CONTACT Hanieh Fattahi hanieh.fattahi@mpq.mpg.de

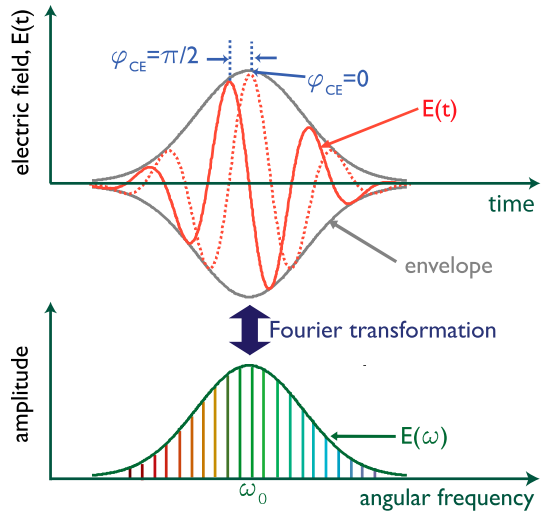

Figure 1. The oscillating electric field of a sub-two-cycle laser pulse at carrier angular frequency ω_0 (top) and the corresponding spectrum (bottom). The gray line shows the amplitude envelope of the electric field and φ_{CE} denotes the carrier-envelope phase offset. The temporal and spectral bandwidth of the pulse are correlated inversely according to the Fourier theory.

$$E(t) = \mathrm{Re}\left[\mathcal{E}(t)e^{-i\omega_0 t}\right]. \tag{4}$$

In case of a few-cycle pulse, where the pulse duration is comparable with the carrier oscillation cycle, propagation can be described by SVEA with some additional corrections [3].

However, defining an envelope for light transients become too ambiguous and a more rigorous approach should be adopted. Lasers and field synthesisers produce waveforms that satisfy the causality principle. Thus, light transients can be described by the complex-valued *analytic signal* $\mathcal{E}_a(t)$, which was initially introduced by Gabor [4]. Requirement of causality has an important mathematical consequence: real and imaginary parts of the analytic signal are connected via the Hilbert transform

$$\begin{aligned}\mathcal{E}_a(t) &= E(t) + i\mathcal{H}[E(t)], \quad \mathcal{H}[E(t)] \\ &= \mathrm{p.v.}\frac{1}{\pi}\int_{-\infty}^{\infty}\frac{E(t)}{t-\tau}\mathrm{d}\tau.\end{aligned} \tag{5}$$

This property is similar to the well-known Kramers–Kronig relations for real and imaginary parts of electric susceptibility [5]. As any other complex function, analytic signal can be represented in a polar form

$$\mathcal{E}_a(t) = f(t)e^{i\varphi(t)}, \tag{6}$$

where $f(t)$ is an *instantaneous amplitude* or *envelope* of the pulse

$$f(t) = |\mathcal{E}_a(t)| \tag{7}$$

and $\varphi(t) \equiv \arg\mathcal{E}_a(t)$ is the *instantaneous phase*. Its first derivative is called the *instantaneous angular frequency*

$$\omega(t) = \frac{\mathrm{d}\varphi(t)}{\mathrm{d}t}, \tag{8}$$

and the second derivative defines the rate of the frequency change [6]

$$c(t) = \frac{\mathrm{d}^2\varphi(t)}{\mathrm{d}t^2}. \tag{9}$$

The concept of carrier-envelope phase can be generalised for the light transients in terms of the so-called *global phase* φ, which is defined as an argument of the *fractional Hilbert transform* [7,8]

$$E(t,\varphi) = \mathcal{H}_\varphi[E(t,0)] = \cos\varphi E(t) + \sin\varphi\mathcal{H}[E(t)] \tag{10}$$

that allows to obtain $E(t,\varphi)$ from the waveform $E(t,0)$, which has the global maximum at the same point as its envelope $f(t)$. Rigorous theory of sub-cycle pulse propagation was developed in Refs. [9–11].

However, why are shorter laser pulses ever desired?

When an electric field of light with the carrier frequency ν_0 ($\omega_0 = 2\pi\nu_0$) and the field amplitude E_0, $E(t) = E_0\sin(\omega_0 t)$, interacts with a medium, it polarises the atoms in the direction of the field, $P(t)$. At low intensities, this polarisation follows the electric field linearly, which is why it is called linear optics. At higher intensities, the linear relation between $P(t)$ and $E(t)$ is broken. For photon energies much smaller than the bandgap of materials, the polarisation response of material is:

$$P(t) = \epsilon_0\left(\chi^{(1)}E(t) + \chi^{(2)}E(t)^2 + \chi^{(3)}E(t)^3 + \cdots\right), \tag{11}$$

where ϵ_0 is the electric permeability of vacuum and different orders of $\chi^{(i)}, i = 1,2,3,\ldots$, correspond to different orders of nonlinear susceptibility. This is the regime of perturbative nonlinear optics, and the contributions of higher order induced polarisation decrease rapidly for a higher order of nonlinear susceptibility. Each term in Equation 11 describes a different nonlinear phenomena. For example, the second term describes second harmonic generation, and the third term describes third harmonic generation as well as the intensity-induced changes of the refractive index (optical Kerr effect).

The efficient generation of high-order nonlinearities demands a higher field amplitude; However, as the laser intensity approaches $10^{14}\,\mathrm{W/cm^2}$ the atomic response deviates from Equation 11 to a new nonlinear regime, a non-perturbative regime.

As shown in Figure 2, at this intensity, the atomic dipole oscillation is greatly enhanced and the laser field is strong enough to suppress the static Coulomb potential

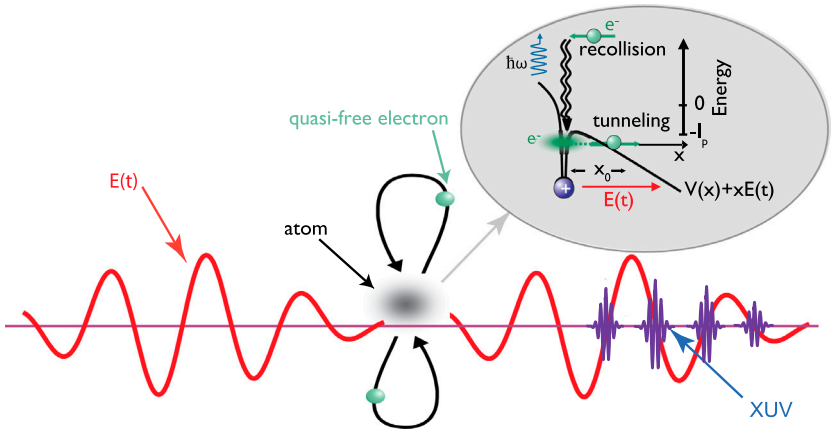

Figure 2. Three-step model of high harmonic generation: Linearly polarised intense laser pulses (E(t)) bend the Coulomb potential (V(x)) of atoms. The most weakly bond electrons tunnel out of the newly formed barrier. The quasi-free electron accelerates in the laser field and returns to its parent ion in the next half-cycle of the laser field. The recombination of electrons into their bound states results in generation of XUV pulses for each half-cycle of the laser pulse ($\hbar\omega_0$).

of the atomic core. This provides the chance for electrons to tunnel out and accelerate in the direction of the laser field. When the next half-cycle of the laser field arrives, the liberated electrons are accelerated back towards their parent ion and recombine. The generation of high-energy photons is the outcome of this recombination, and the process is called high harmonic generation (HHG). The highest energy photon (cut-off) generated in the HHG process scales linearly with the laser intensity and inverse quadratically with the carrier frequency of the laser [12]:

$$E_p = I_p + 3.17\frac{e^2{E_0}^2}{4m_0{\omega_0}^2}, \tag{12}$$

where I_p is the ionisation potential and m_0 and e denote the free electron mass and elementary charge, respectively.

For a laser pulse with several optical cycles, photoionisation takes place at each half-cycle of the laser field. Therefore, the ground state of atoms could become depleted before the arrival of the laser field's main peak.

In HHG, isolated attosecond pulses with the highest photon energies are generated only by the most intense half-cycle of the laser. Other half-cycles of the laser field with lower amplitude produce multiple attosecond pulses containing lower photon energies. These pulses are not isolated anymore as multiple half-cycles contributed in their generation.

Producing broadband-isolated attosecond pulses requires an attosecond light switch to effectively turn on the HHG process during only one half-cycle of the laser field. These requirements are satisfied by driving the HHG utilising single- or sub-cycle light transients at long carrier frequencies, confining photoionisation to a single half-cycle and making it possible to scale the laser intensity without pre-depletion of the ground state.

In the following, I discuss the design and the current status of an apparatus that fulfills the above-mentioned criteria. The machine is based on the perturbative nonlinear optical phenomena to provide a platform for extending non-perturbative nonlinear optics to new frontiers on a laboratory scale, meaning the generation of photons with keV energy and attosecond pulse duration.

2. State of the art

The first insight into nonlinearity in relation to optical frequencies happened one year after the invention of lasers [13]. Franken et al. observed the generation of the second harmonic of the ruby laser in a quartz crystal [14]. This experiment was the first demonstration of nonlinear optics in a perturbative regime and opened up a new avenue in light–matter interaction. The profound theoretical basis for this new regime, provided by Bloembergen et al., suggested that increasing the peak power of the incident laser field results in the generation of higher order nonlinearities in material [15]. These findings initiated a half-century of research towards increasing the peak power of lasers by reducing their temporal pulse duration or equivalently increasing their output energy. At the same time, pulses at repetition rates of several kHz or higher are desired to reduce the measurement time.

In 1985, the first few-cycle pulses were generated in a passively mode-locked organic-dye laser [16]. Thereafter, in 1987, the barrier of sub-ten fs laser pulses was broken by extracavity pulse compression of dye lasers [17], reaching tens of megawatts of peak power [18,19]. Achieving higher average and peak power with dye-laser technology was not possible, as it led to the evaporation of the organic-dye gain medium. This encouraged laser physicists to move towards a solid-state gain medium.

The invention of titanium-doped sapphire (Ti:Sa) lasers and multi-layer chirped mirrors [20,21] along with the discovery of Kerr-lens mode-locking (KLM) by Sibbett in 1991 [1] allowed the generation of sub-ten fs pulses directly from a Ti:Sa oscillator [22,23].

However, energy scaling of these few-fs pulses seemed to be impossible due to their high peak power, which was close to the damage threshold of the laser gain media. The demonstration of chirped pulse amplification (CPA) [24] in optical frequencies by Mourou et al. [25] paved the way towards boosting the peak power of few-cycle pulses by several orders of magnitude, reaching 1 PW at 1 Hz repetition rates (BELLA at Berkeley Lab in USA) and 1.5 PW at 0.1 Hz repetition rates (CoReLS laser system in South Korea). The external spectral broadening of few-cycle, mJ-level pulses of a CPA-based amplifier in a hollow-core fiber (HCF) and their subsequent pulse compression, in addition to the ability of scientists to control the carrier-to-envelop phase (CEP) of few-cycle pulses [26], resulted in the demonstration of the first isolated attosecond pulses and emergence of an entirely new research field, attosecond physics [27].

Pulses broadened in a HCF were compressed to 4 fs at 800 nm carrier wavelength [28], although the generated spectrum supported a shorter pulse duration. This deficiency was due to the limited spectral bandwidth of chirped mirrors to one-octave. Other pulse compression techniques such as spatial light modulation support broader bandwidth but their operation is limited to pulses with low peak powers [29]. Because of excessive ionisation and thermal instabilities in a HCF, the achievable peak and average power from these few-cycle pulse generators is limited to approximately 1 TW and 10 W, respectively [30,31].

In 2011, short-pulse generation entered a new regime, called optical light transients [32]. Wirth et al. overcame the limitation of chirped mirrors in spectral bandwidth by decomposing the super-octave spectrum from the HCF into several spectral regions. After compressing each of the spectral regions by using chirped mirrors, different spectral components were coherently superimposed to create sub-cycle light transients. This super-octave light transient of synthesised visible-infrared light provided unprecedented flexibility for steering light–matter interactions and is capable of triggering and probing electron dynamics with sub-femtosecond precision, even without the use of attosecond extreme ultra-violet (XUV) pulses [33–35]. However, the low average as well as peak power of these light transients [35,36] constitutes a major limitation for widespread use of this extreme form of optical radiation. Moreover, the central frequency of these light transients is currently limited to the near-infrared spectral range.

In parallel to advances in CPA-based amplifiers, Dubietis et al. were able to show the amplification of 70 fs pulses by a factor of 10^4 in 1992, harvesting the second-order nonlinearity of BBO in an optical parametric chirped pulse amplifier (OPCPA) [37]. Afterwards, the demonstration of mJ- to J-energy-level few-cycle pulses [38–41] at different carrier frequencies using OPCPA made this technique a promising path towards boosting the energy and average power of few-cycle pulses. However, the spectral bandwidth of the gain in OPCPA is limited by the phase-matching between the interacting pulses in the nonlinear medium. In recent years, progress in OPCPA suffered from the lack of turn-key, powerful, efficient and cost-effective pump lasers.

To date, advances in Yb-doped lasers in fiber [42], slab [43,44], or thin-disc [45,46] geometry have started to fulfill the criteria for suitable pump sources for OPCPA and holds promise to change the current state of the art of OPCPAs to few-cycle pulses with higher energy and average power.

In addition to simultaneous scalability in energy and average power, the next generation of laser sources should be flexible in terms of the carrier frequency, while containing a one- or sub-cycle electric field. The nonlinearity induced by such a giant peak power of laser transients will open up new regimes of light–matter interaction. As the damage threshold of materials scales inversely with the square root of the pulse duration, matter can be irradiated with such transients to intensities beyond the current optical breakdown of materials, opening the possibility to explore new regimes of nonlinearity.

The merge of four existing technologies is discussed below: (a) the generation and metrology of phase-stable coherent supercontinua, (b) Yb-doped laser technology, (c) broadband OPCPA, and (d) interferometrically stable super-octave waveform synthesis. Combination of these concepts hold promise to provide high-energy, high-repetition-rate, ultra-broadband light pulses as a versatile platform for studying the new regime of nonlinearity in matter in the coming years.

3. Next-generation light sources

3.1. How to boost the photon energy?

Two phenomena can result in the efficient amplification of photon energies: stimulated emission in a resonator and optical parametric amplification (OPA). In the first case, the stored energy in an optically or electronically pumped gain medium can be released via stimulated emission, leading to the amplification of photons. Here, the amplification gain is limited to amplified spontaneous emission (ASE) that happens simultaneously in the gain medium. The carrier frequency of the amplified spectrum

is dictated by the energy-level structure of the active laser medium and is limited by gain narrowing during amplification.

OPA, however, is a non-resonant, instantaneous, perturbative nonlinear process where the energy of a high-energy pulse is transferred to a low-energy pulse harvesting the second-order nonlinearity of materials.

In the wave picture of light, the process is described by considering the superposition of two fields with the carrier frequencies ν_p (pump) and ν_s (signal/seed), which causes a modulation with a frequency of $\nu_p - \nu_s$ on the intensity envelope of the superimposed electric field. In interaction with a nonlinear medium and in the presence of a small perturbation on the envelope of the input field, a third electric field with the carrier frequency $\nu_i = \nu_p - \nu_s$, called idler, is generated (Figure 3(a)).

From a quantum-electrodynamics point of view, the interaction between a nonlinear medium and a high-energy, non-resonant pump photon with frequency ν_p excites the medium to a higher energy virtual level. The virtual excited population returns to the ground state nearly instantaneously. In the presence of a signal photon with frequency ν_s a stimulated decay may occur. Due to the conservation of energy during this process two new photons with energies of $h\nu_s$ and $h\nu_i = h\nu_p - h\nu_s$, are generated (Figure 3(b)).

The gain bandwidth of OPA is limited by absorption and phase-matching conditions of the interacting pulses and is dictated by the conservation of momentum:

$$k_p - k_s - k_i = 0, \tag{13}$$

where k_p, k_s, and k_i are the wave vectors of the pump, signal and idler, respectively. During propagation in the material, the amplification bandwidth will be limited to the group velocity slippage of the interacting pulses. Therefore, a broad amplification bandwidth can be achieved by minimising the group velocity mismatch between the interacting pulses, which can be tuned by crystal type, thickness, orientation, temperature and the geometry of the interacting beams. Therefore, amplification bandwidth is inversely proportional to the crystal thickness, as pump, signal and idler pulses become separated during longer propagation length, due to the natural dispersion in the material.

In degenerate optical parametric amplifiers (DOPA), materials with zero group velocity dispersion at the carrier frequency of the idler and signal are used to minimise the group velocity mismatch between both beams and to maximise the amplification bandwidth [48]. However, because the SHG of the signal is also phase-matched in DOPA, an unwanted backward flow of energy from the signal to the pump occurs, which modifies the shape of the amplified spectrum and limits the conversion efficiency.

For amplifying frequencies away from the zero group velocity dispersion point, the group velocity mismatch is minimised by using a geometric trick. Here, the signal pulses are forced to travel a longer distance in the crystal when a noncollinear angle is added, and the temporal interaction length of interacting beams is therefore increased (Figure 3(c1) and (c2)). These types of OPA are called NOPA, which stands for noncollinear optical parametric amplifier [49]. In this case, the generated idler becomes angularly chirped to fulfil the phase-matching condition:

$$\nu_{gs} = \nu_{gi} \cos(\Omega), \tag{14}$$

where Ω is the angle between idler and signal.

Besides the above-mentioned phase-matching techniques, quasi phase-matching can be used where the phase mismatch is compensated by periodically inverting the orientation of the crystal axis [50]. However, the fabrication of such crystals is limited to a few millimetres in aperture and is not applicable to high-energy OPA systems.

In 2014, Schmidt et al. demonstrated the amplification of two-cycle pulses using a new concept called FOPA, or Fourier optical parametric amplification. In FOPA, the broadband signal pulses are spectrally dispersed in space, unlike OPCPA where the seed pulses are dispersed in time, and each spectral region is amplified in different crystals. This approach relaxes the phase-matching requirements for the crystals, but the overall amplification bandwidth is limited to the gratings used for dispersion. In addition, multi-stage amplification employing this approach is immensely complex [51]. Therefore, OPCPA appears to be the most promising technique for the simultaneous scaling of peak and average power, with its amplification gain limited to the amplification of parametric fluorescence, a spontaneous decay of high-energy photons to two photons with lower energy that occurs at high intensities inside the crystal.

3.2. Suitable pump sources

To achieve an optimum conversion efficiency in an OPA, the low-energy seed pulses and high-energy pump pulses should have an optimum spatio-temporal overlap. Employing short pulses to pump an OPCPA simplifies the temporal stretching and compression. In addition, short-pump pulses allow a higher peak intensity in the nonlinear medium [52]. The high pump intensity makes it possible to achieve the required gain in a shorter crystal, allowing a greater amplification bandwidth and less transverse spatial walk-off between the interacting beams.

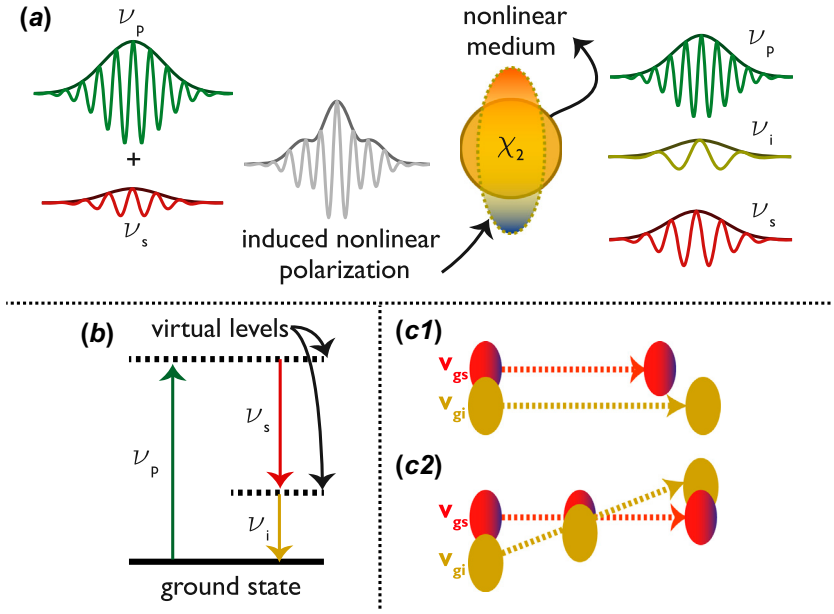

Figure 3. (a) The wave picture of OPA. The superposition of a high-energy pump field with the frequency of ν_p and a low-energy signal field with the frequency of ν_s in a medium with second-order nonlinearity results in the amplification of the signal field and the generation of a new field with the frequency of ν_i, called an idler. (b) The photon-picture of the OPA process, where the high-energy pump photons excite the medium to virtual levels. The presence of the signal photons brings the medium to its ground state while the pump photons are split into signal and newly generated idler photons. (c1) Group velocity mismatch between signal and idler and (c2) the compensated group velocity mismatch in noncollinear geometry [47].

However, the temporal walk-off relative to the pulse duration increases for short pulses. A simple analytical analysis shows that the optimum pump pulse duration to achieve a high conversion efficiency and a broadband gain is around 1 ps [47].

Nevertheless, all these advantages of short-pulse-pumped OPCPA remain useless without an efficient, reliable and powerful pump source. Such pump lasers are required to deliver high-energy near-1-ps pulses with near-diffraction-limited beam quality at repetition rates in the kHz to MHz range, conditions that are met by diode-pumped Yb-doped lasers in fiber, slab, or thin-disc geometry [45].

Currently, Yb:YAG fiber lasers deliver 2 kW of average power at 100 µJ of energy [54], and their energy is scaled to 1.3 mJ at 530 W by coherent combination [55]. In slab geometry, Yb-doped lasers are capable of delivering 1.1 kW pulses at 55 µJ [56]. Cryogenic composite thin-disc lasers reach 100 mJ at 25 W [44]. However, the highest reported average power and energy belongs to a CPA-based Yb:YAG regenerative amplifier in thin-disc geometry, delivering 200 mJ of energy at 1 kW of average power for 1 ps pulses [57].

Here energy and average power scaling are made possible by chirped-pulse-amplification and efficient heat removal from the gain medium, respectively. In this geometry, the gain medium consisting of a Yb:YAG thin-disc with a thickness of hundreds of micrometres is fixed onto a water-cooled diamond substrate. Owing to the efficient heat removal, this geometry allows for high pump power densities exceeding 10 kW/cm^2 but at the expense of a low single-pass gain of typically 10% (small signal) due to the small thickness. However, enough amplification can be achieved by multiple passes through the gain medium or serial combination of several discs as it is shown in Figure 4(a).

In the Yb:YAG thin-disc regenerative amplifier shown in Figure 4, low energy seed pulses from a Yb:YAG oscillator or a Yb:YAG fiber amplifier centred at 1030 nm are stretched to several hundreds of ps using a grating pair. Afterwards they are coupled into the laser cavity and pass through the laser gain medium more than 100 times. This corresponds to kilometres of beam path. At each round trip, the pulse is amplified further. When the amplification saturates, the pulses are coupled out by using an electro-optic switch, in this case a Pockels cell, and sent to a grating compressor for pulse compression (Figure 4(b) and (c)). A typical spectrum of a Yb:YAG thin-disc regenerative amplifier, its temporal profile after compression, its spatial profile, and its power stability over several hours of operation are shown in Figure 5 [53].

This unique performance, in combination with the reliability of industrial lasers, makes Yb:YAG lasers

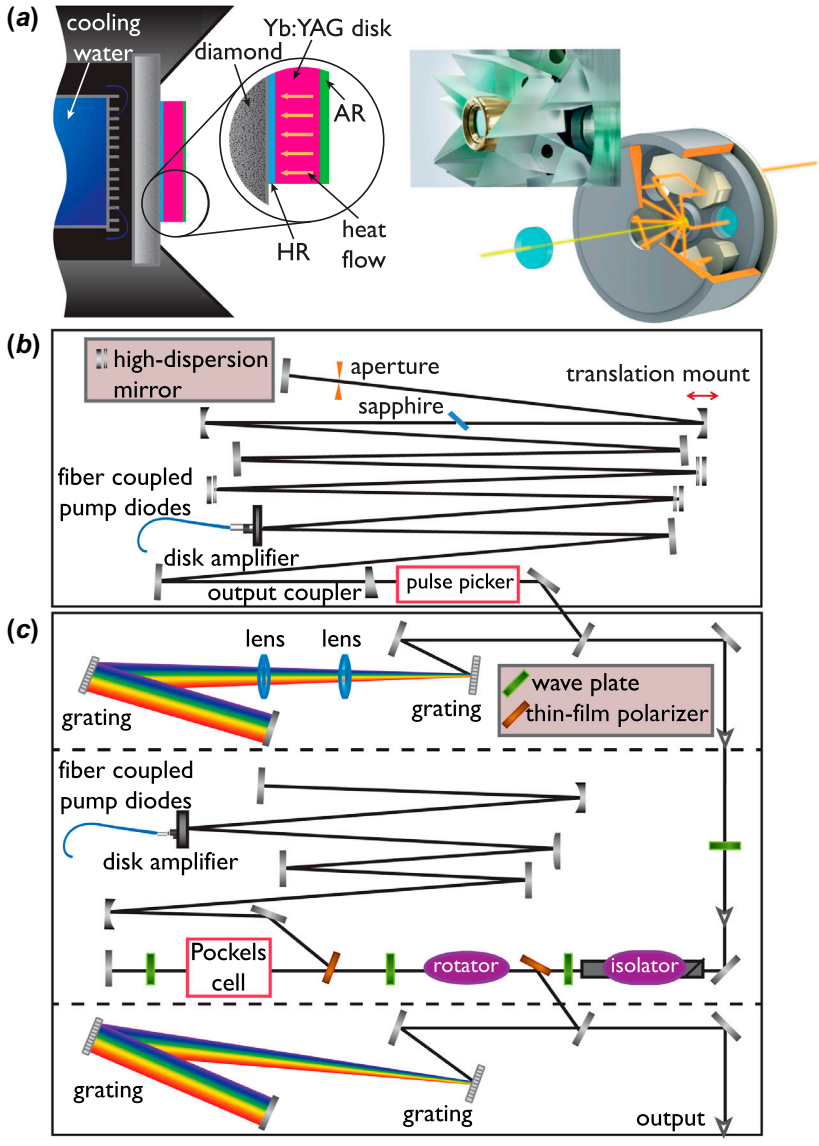

Figure 4. (a) Basics of thin-disc laser technology. A thin Yb:YAG disc is mounted on a diamond substrate that is cooled from the back side. The heat removal from the bonded disc on the substrate is very efficient as the disc is about 100 μm-thick (left). Pump-light reimaging technique in the thin-disc gain medium is used to compensate for the low pump absorption in the gain medium (right). Courtesy of Thomas Metzger. (b) Layout of a KLM thin-disc oscillator. These type of oscillators deliver μJ-level pulses at MHz repetition rates and few hundred fs pulses. (c) Typical schematic of Yb:YAG thin-disc regenerative amplifier. The seed pulses from the Yb:YAG oscillator are temporally stretched to several hundred ps before entering the amplifier. The regenerative amplifier contains a fiber-coupled diode laser to pump the Yb:YAG thin-disc gain medium, an electro-optic switch, or Pockels cell to couple out the amplified pulses, and a pair of dielectric gratings for temporal pulse compression down to 1 ps [53].

potential drivers for multi-channel broadband OPCPA systems where different harmonics of the laser can be used to pump different spectral regions.

3.3. OPCPA-based field synthesiser

The basic architecture of the proposed next generation sub-cycle light sources (Figure 6) consists of (i) a powerful pump source, in this case a Yb:YAG thin-disc regenerative amplifier, (ii) a CEP-stable multi-octave seed generated directly from the Yb:YAG amplifier, (iii) super-octave beam splitter to divide the generated super-octave spectrum into several spectral regions, (iv) multi-stage, multi-channel optical parametric amplifiers for amplification of the complementary portions of the supercontinuum, (v) pulse compression of each channel into few-cycle pulses, and finally, (vi) a coherent recombination of the output of these channels. Here the fundamental (at 1030 nm), second harmonic (at 515 nm) and third harmonic (at 343 nm) of a Yb:YAG thin-disc regenerative amplifier can be used to pump few-cycle OPCPAs in mid-infrared (MIR) spectral regions centred at 2 μm,

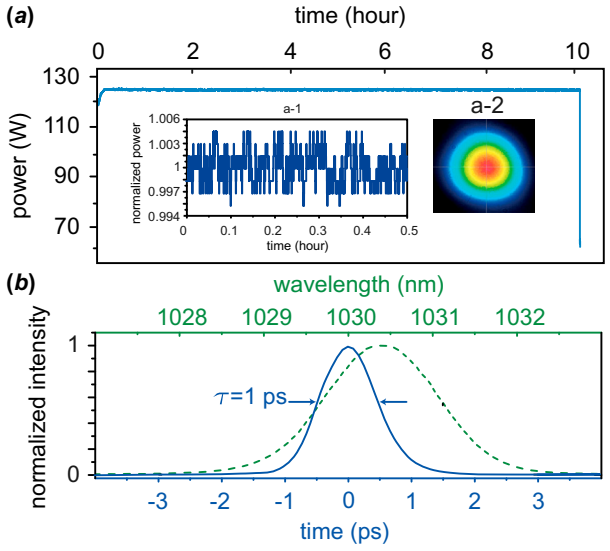

Figure 5. (a) Power stability of a 20 mJ, 100 W, 1 ps, Yb:YAG thin-disc regenerative amplifier over 10 hr continuous measurement. Inset: (a-1) Normalised power over half an hour of operation. (a-2) Output beam profile of the laser. (b) Spectral (green) and temporal (blue) profile of the 1-ps laser pulses [53].

near-infrared (NIR) spectral regions centred at 1 μm, and visible (VIS) spectral regions centred at 550 nm.

A CEP-stable super-octave spectrum from the Yb:YAG amplifier can be generated by difference-frequency generation (DFG) as an inherently phase-stable process in combination with self phase-modulation-induced spectral broadening. The direct generation of broadband seed pulses from pump pulses assures a minimum temporal jitter between pump and seed pulses in the amplification chains and removes any need for an additional synchronisation stage [59,60]. As waveform synthesis enables control over the electric field of femtosecond pulses on a sub-cycle scale, it therefore requires an initial coherent supercontinuum seed with absolute phase stability.

In an experiment demonstrated by Fattahi et al. [58], super-octave seed pulses were generated directly from a Yb:YAG thin-disc amplifier. In this scheme, a small fraction of the 1-ps pulses of the Yb:YAG thin-disc amplifier were shortened to 650 fs in a cross-polarised wave generation (XPW) stage [61]. The shortened XPW pulses possessed an excellent temporal contrast. This step was essential to generate a stable filament in bulk in the subsequent stage, as the material damage threshold and critical peak power for 1-ps-driven continuum generation in bulk (in this case, a 4-mm YAG crystal) are of the same order of magnitude. A narrow spectral region of the generated continuum, centred at 790 nm, was amplified in a saturated OPCPA stage in order to boost the energy and to filter intensity fluctuations caused by the preceding third-order processes. Mixing these amplified pulses with the pulses from the thin-disc amplifier in a BBO difference frequency generator resulted in CEP-stable pulses ranging from 1700 to 2200 nm. The spectrum of this output was extended to the visible spectral range by self phase modulation in a 6 mm YAG crystal after temporal compression (Figure 7). The CEP-stable supercontinuum was divided into three spectral regions [62] of comparable bandwidth in the VIS, NIR and MIR in order to seed the respective few-cycle OPCPA channels, as shown in Figure 6.

Simulated OPCPA spectra of a three-channel OPCPA system are shown in Figure 8. In this simulation 200 mJ of energy of a Yb:YAG pump laser is distributed amongst the three pump wavelengths as follows: 40 mJ at 343 nm, 74 mJ at 515 nm and 86 mJ at 1030 nm for pumping the VIS, NIR and MIR channels of the OPCPA system, respectively. Amplification in a 4-stage OPCPA containing four subsequent $LiNbO_3$ crystals as the nonlinear medium can yield 19 mJ pulses at 12 fs for the MIR channel (Figure 8, orange curve). 5 fs pulses can be amplified up to 23 mJ of energy in the 4-stage second-harmonic-pumped NIR channel, employing LBO crystals (Figure 8, red curve). Finally 5 fs pulses with 7 mJ of energy can be achieved by using 40 mJ pulses at 343 nm to pump BBO crystals in a 3-stage OPCPA chain (Figure 8, blue curve).

The spectral coverage of the waveform synthesiser can be readily extended to the far-infrared by intrapulse DFG driven by the compressed output of the MIR OPCPA channel. The simulation predicts a continuum spanning from 4 to 20 μm when using a single LGS nonlinear crystal driven by a few-cycle 2 μm pulse, with a conversion efficiency as high as several per cent. The simulated DFG spectrum and its electric field are shown in green in Figure 8.

The amplified pulses of all channels can be individually compressed and combined by a dichroic beam combiner to synthesise sub-cycle to few-cycle near-infrared to visible waveforms and, after a further frequency conversion to reach out into the far-infrared range, infrared waveforms spanning the range of 0.7–20 μm.

Figure 8(b) shows the first experimental demonstration of the amplified spectra of the first stages of the NIR and MIR OPCPA channels of such a synthesiser. The super-octave spectrum shown in Figure 7 and the Yb:YAG amplifier discussed in 3.2 and shown in Figure 5 were used to seed and pump the two OPCPA channels, respectively. Both channels contain 15 μJ of energy.

3.4. Coherent synthesis and keV photon generation

The three-channel few-cycle OPCPA prototype system described above offers a conceptually simple route to

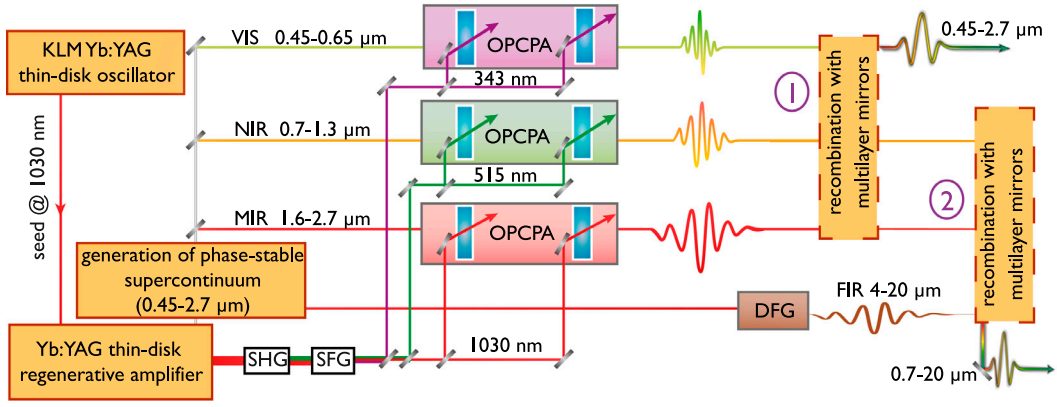

Figure 6. Proposed schematic architecture of a three-channel OPCPA field synthesiser seeded and pumped by picosecond Yb:YAG lasers (see: 3.2). A part of the output of the Yb:YAG amplifier is used for generating a phase-stable multi-octave supercontinuum seed, which is then split into three channels, centred at 550 nm, 1 μm and 2 μm, respectively. The different channels are pumped by different low-order harmonics of the multi-mJ level kHz, Yb:YAG regenerative amplifier output. Each channel supports few-cycle pulses. By coherently combining the three few-cycle channels, light transients spanning from 0.45 to 2.7 μm can be generated (1). The sub-cycle waveforms can be furthermore extended to far-infrared by DFG of the seed pulses (2) [58].

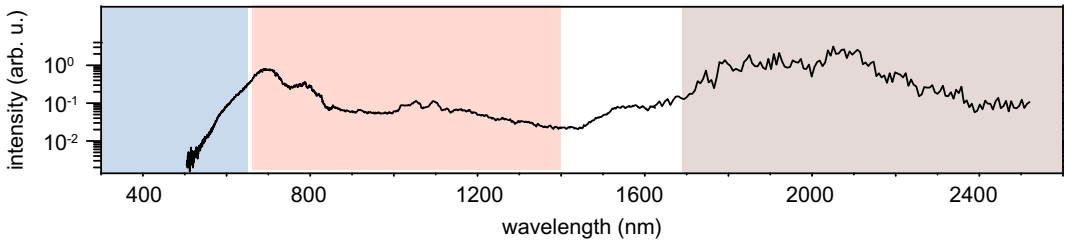

Figure 7. CEP-stable super-octave spectrum directly generated from a 1-ps Yb:YAG thin-disc regenerative amplifier [58].

scaling multi-octave optical waveform synthesis to the multi-terawatt regime. In coherent synthesis of few-cycle pulses, fine control over the spectral phase, the relative phase of each pulse, and their relative timing jitter are crucial. For this purpose, the amplified pulses at each OPCPA channel are sent to delay stages to control the relative phase of each arm. Afterwards, each amplified pulse is compressed to its Fourier transform limit supporting few-cycle pulses by employing a chirped-mirror compressor. Finally, the compressed pulses are combined and coherently superimposed by using two broadband dielectric beam combiners. Changing the relative amplitude and relative timing of the three pulses can result in a great variety of sub-cycle optical light transients. The simulated OPCPA's spectra of the proposed synthesiser, shown in Figure 8(a), were used to simulate three different light transients, by changing the relative amplitude and phase of the OPCPA channels analytically. The results are shown in Figure 9.

As with any kind of interferometer, relative timing fluctuations between the three arms of the synthesiser should be suppressed to achieve a stable light transient. Here, as each of the pulses contains an electric field with just two or three cycles, relative timing drifts have to be compensated to a fraction of the half-field cycle. The intrinsically CEP-stable OPCPA seed, in combination with a balanced optical cross-correlator [65] for temporal drift compensation, ensures a stable transient at the synthesis point (Figure 9).

The generated light transient can be optimised to extend HHG into the keV regime. The generation of isolated attosecond pulses with the highest possible photon energy ideally calls for a waveform consisting of two strong half-cycles of the electric field, one for pushing electrons away from their parent ion and a second for pulling them back. As discussed earlier, driving pulses with more than two half-cycles causes undesirable pre-ionisation in the interaction medium, reducing XUV production efficiency by reduced phase-matching and/or depletion of the ground state. Moreover, a Gaussian single-cycle waveform unavoidably truncates the achievable cut-off energy, as the relative amplitude of each half-cycle is fixed to a sinusoidal shape. Tailored multi-octave transients are capable of circumventing this problem, as the required half-cycles can be turned on much more abruptly thanks to the available bandwidth, allowing an efficient maximisation of harmonic photon energy. In addition, the abrupt turn-on of the intense cycle efficiently suppresses pre-ionisation, resulting in a higher keV harmonic yield.

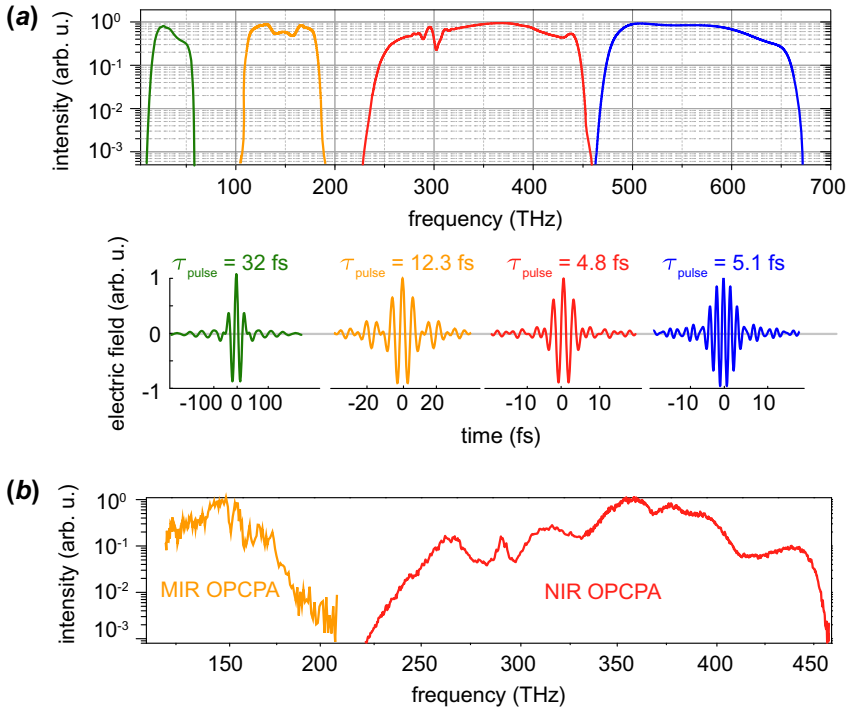

Figure 8. (a) Amplified spectra (top) and the corresponding waveforms (bottom) of the synthesiser's three channels obtained from the simulation with: blue for the visible channel, red for near-infrared, orange for mid-infrared and green for the extension to the far-infrared. All individual channels support few-cycle pulses [47]. (b) The first Experimental demonstration of the amplified spectra of the NIR and MIR channels of the waveform synthesiser. In the NIR channel amplification was done in a 4 mm LBO crystal, pumped by 1 mJ at 515 nm. In the MIR channel 1 mJ at 1030 nm was used to pump a 2 mm thick periodically poled LiNbO3 (PPLN) crystal [58].

The cut-off energy in HHG also depends on the energy distribution between the spectral components of the transient. Low-frequency photons tend to extend the cut-off energy although high-frequency photons are desired for the ionisation process despite tending to reduce the cut-off energy. Therefore, adding a selectively introduced chirp to the transient in order to shift the high-frequency photons of the VIS channel of the synthesiser to the leading edge of the transient, where the first half-cycle is required to ionise the atom, should extend the cut-off energy even further [47].

Figure 10 shows the calculated dipole response of a single He atom for different transients at a peak intensity of 50×10^{14} W/cm^2, for the three cases of (i) zero spectral chirp and uniform spectral density, (ii) zero spectral chirp and optimised spectral density, (iii) optimised chirped and optimised spectral density. It can be seen that the third case results in the highest cut-off energy amongst others. Here the spectral density of the transient is optimised in favour of low-frequency photons, resulting in more amplification of the MIR channel relative to the NIR and VIS channels in the OPCPA chain. Additionally, high-frequency photons are selectively moved to the leading edge of the transient by adjusting the relative temporal delay of the VIS channel to the MIR and NIR channels.

For such laser fields with large amplitude, the magnetic field of the laser will become large enough to affect the trajectories of the liberated electrons via Lorentz force, and relativistic effects set in. Consequently, the probability of an electron's recombination with its parent ion and hence the efficiency of HHG will be reduced. However, at the field amplitudes considered for the above-mentioned simulation, the magnetic drift of the electrons is still at a tolerable level.

Figure 11 summarises the results of preliminary numerical studies aimed at finding the optimum light transient available from the discussed apparatus for isolated attosecond pulse generation with the highest possible efficiency at keV photon energies. The best light transient which has been found so far does indeed exhibit the features described above: a light transient carrying most of its energy in a single intense wave cycle, which is turned on as abruptly as possible with the available spectral bandwidth. With this optimised light transient the photon energy of a single attosecond pulses reaches 2.5 keV, a new regime that has not been possible so far.

4. Outlook

Direct observation and the understanding of electronic motion near the atomic core is a long-standing dream

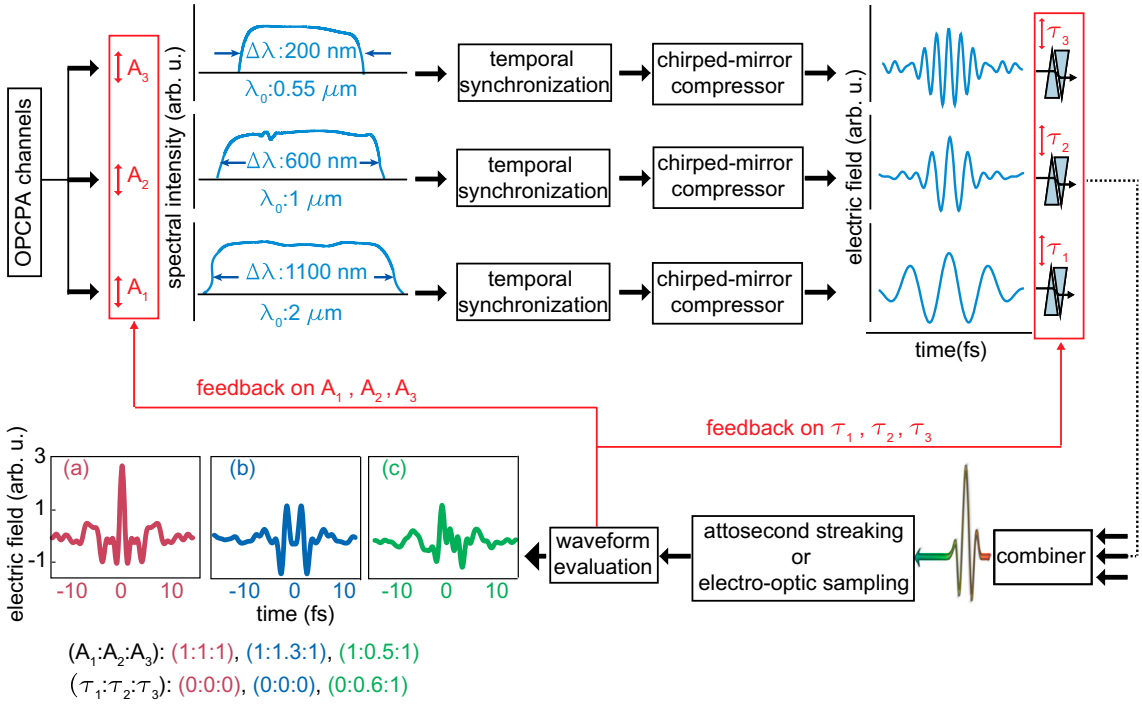

Figure 9. Detailed set-up of the temporal synthesis of the VIS, NIR and MIR pulses. The amplified spectra of all three OPCPA channels centred at 0.55 μm, 1 μm, and 2 μm are first sent through a delay line to Achieve a temporal overlap between the synthesiser's three arms. Thereafter the temporally synchronised pulses are compressed to their Fourier transform limit in each arm separately using a set of broadband dielectric chirped mirrors. After passing through a pair of glass wedges to fine-tune the relative delay between each arm the three compressed pulses are spatially combined in two broadband dielectric beam combiners. The generated light transients are evaluated using attosecond streaking [63] or electro-optic sampling [64]. By adjusting the relative spectral amplitude of each arm (A_1, A_2, A_3) and their relative phase (τ_1, τ_2, τ_3), a variety of transients can be generated. As an example, panels (a), (b) and (c) show three differently synthesised transients.

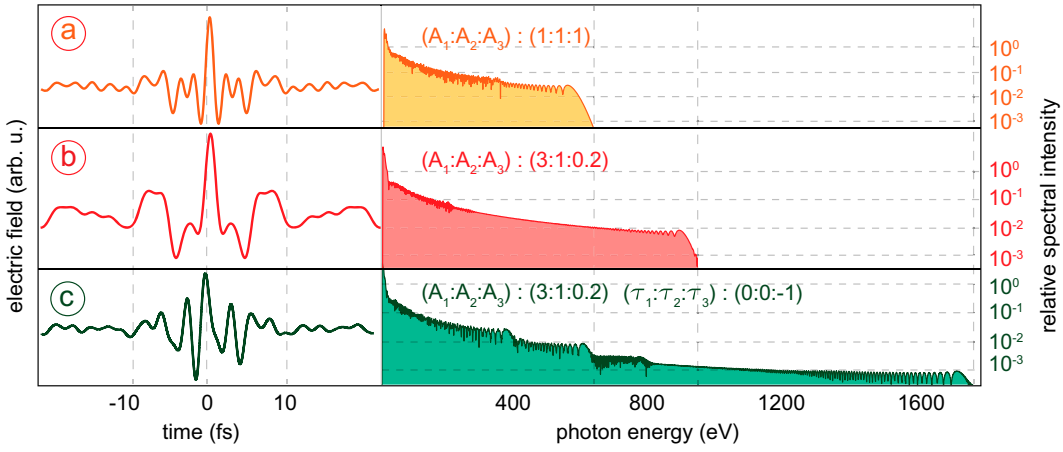

Figure 10. Right panel: Simulated HHG spectra of a single He atom at a peak intensity of 50×10^{14} W/cm^2 for different light transients. (A_1:A_2:A_3) represents the relative amplitude and (τ_1:τ_2:τ_3) represents the relative temporal delay of the (MIR:NIR:VIS) channels. Left panel: Corresponding transients of the synthesised pulses [47].

of physicists. Applying this knowledge to examine the interaction of charge carriers within solids and their relaxation mechanisms could open paths to new technological applications in information processing and ultrafast electronics.

The heart of attosecond spectroscopy [27] lies in advancing our understanding of atomic-scale electron motion [66,67] and provides access to dynamic changes in the atomic and electronic structure of matter. Attosecond temporal resolution has enabled the direct measurement

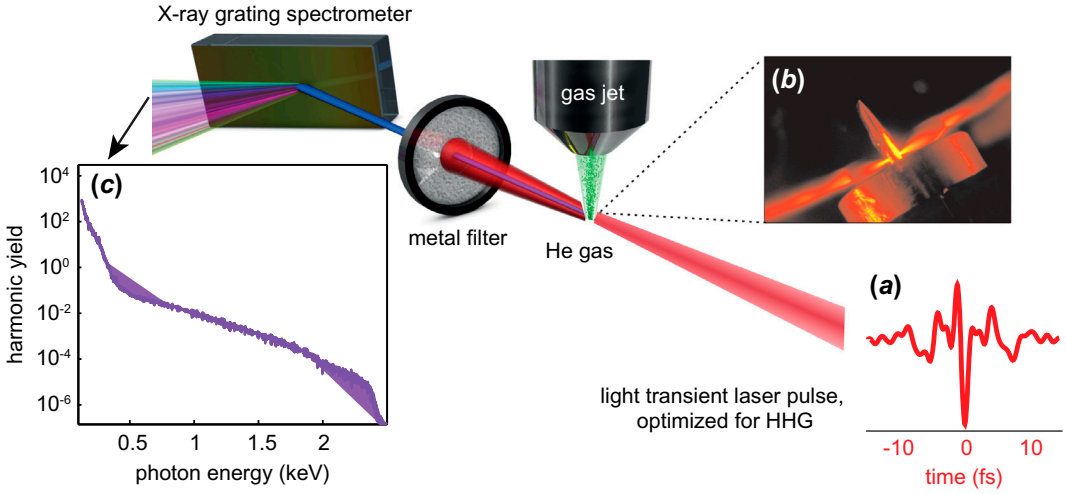

Figure 11. Schematic of a proposed attosecond metrology beamline. The optimised light transients (a) are focused into He gas (b) at a peak intensity of 50×10^{14} W/cm^2 to generate isolated attosecond X-ray pulses. The metal filter is used to separate the generated attosecond pulses from the light transient. The HHG spectrum from such a light transient, obtained from the simulation (c) extends to 2.5 keV photon energy and X-ray regime. Image of HHG gas nozzle: courtesy of Ferenc Krausz.

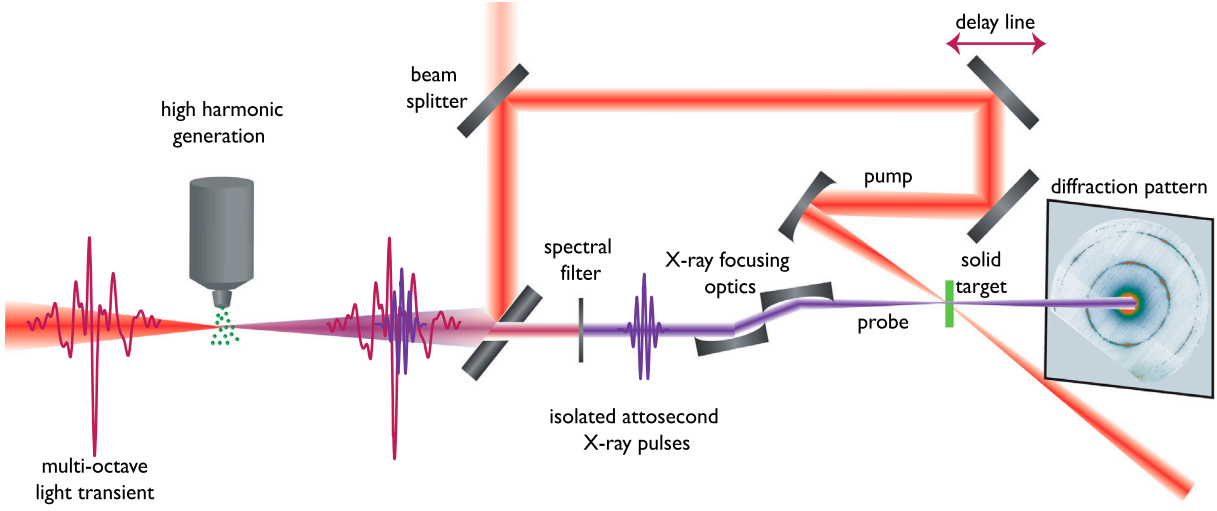

Figure 12. Proposed sketch of the X-ray diffraction, attosecond spectroscopy Set-up. The optimised light transient for HHG is focused into a noble gas to generate X-ray attosecond pulses. The filtered X-ray pulses and the light transient are separated spatially by using a pierced mirror and a metallic filter. Thereafter the X-ray pulses are focused to a solid sample for probing the electron dynamics of the solid, while the light transient is used to excite electrons in the target. By changing the relative delay between the pump and probe arms, and recording the X-ray diffraction pattern of the sample, a four-dimensional movie of the electron dynamics can be reconstructed.

of fundamental processes, such as electron tunnelling [68], electron wave packet dynamics [69] and photoemission [70].

X-ray diffraction microscopy is capable of reconstructing the three-dimensional stationary atomic structure of solids or molecules as well as the distribution of electrons inside atoms.

Therefore, a complete picture of the electrodynamics in solids, with subatomic resolution in space and time, is possible by combining X-ray diffraction and attosecond spectroscopy. Analytical studies suggest that the instantaneous charge distribution in matter can be probed by attosecond pulses [27] producing a diffraction pattern, and the movement of the electrons can be recorded by varying the arrival time of the X-ray pulses with attosecond resolution. Consequently, it could be possible to record freeze-frame snapshots with picometre spatial resolution and attosecond exposure time, creating a four-dimensional (4-D) movie of the evolution of electrons in solids.

The current generation of 4-D imaging is unable to access atomic-scale electronic rearrangements in solids

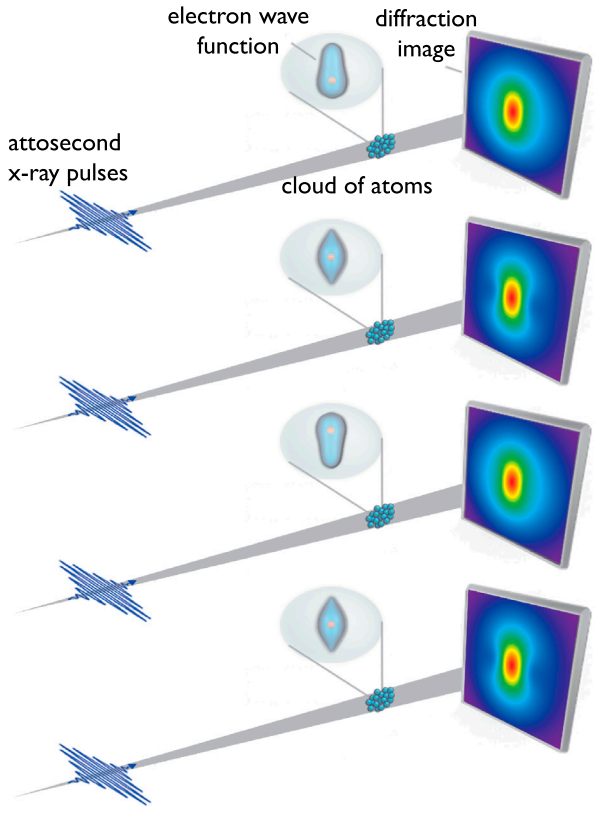

Figure 13. Attosecond X-ray diffraction: As a coherently induced charge oscillation takes place in an atom or molecule, an incident X-ray pulse takes a diffraction snapshot of the electron distribution at the time of interaction; changing the time delay between the source of the excitation and the attosecond pulse allows for the temporal evolution of the charge density to be directly measured in time and space. The figure represents the simulated dynamic of hydrogen atoms when they are exposed to 100-as, X-ray pulses and are excited into the 1S-2P coherent superposition state. As it is shown the electron dynamic can be reconstructed by means of X-ray diffraction, attosecond spectroscopy [27].

and molecules. Time-resolved X-ray diffraction that has been implemented with X-rays from laser-produced plasmas has a sub-picosecond temporal resolution [71]. X-ray pulses from large-scale facilities such as synchrotrons are also limited to picosecond temporal resolution. Generated X-ray photons from free electron lasers (FEL) only support femtosecond temporal resolution and they have a different pulse-to-pulse, pulse duration [72].

Moreover, the external synchronisation of FEL with a fs laser source is cumbersome and limited to the temporal jitter between the two laser sources. Electron time-resolved diffraction microscopy [73–75] as an alternative provides picometre spatial resolution but is also limited to fs temporal resolution [76–78]. Therefore, there is a demand for a table-top source that generates isolated attosecond X-ray pulses.

Existent isolated attosecond pulses provide subatomic time resolution limited to nanometre spatial resolution. Ti:Sa-based attosecond sources produce spectroscopically useful photon fluxes limited to photon energies of 180 eV [31]. These pulses have a wavelength of 6.8 nm, enabling resolution of charge movement on a scale of tens of nanometres. However, the short wavelength of attosecond pulses holds equal potential for high spatial resolution imaging if it can be extended to X-ray photons.

Hence, the real-time observation of electronic changes calls for attosecond temporal resolution to be combined with the subatomic spatial resolution. A proposed schematic of such a pump-probe apparatus is shown in Figure 12. The attosecond keV X-ray pulses enabled by the described apparatus constitute an ideal light source for observing the evolution of charge polarisation in excited solids with picometre resolution in space and attosecond resolution in time. This method may elucidate electron dynamics in inner shells; thus opening the door for time-resolved intra-nuclear dynamics (Figure 13).

The isolated keV attosecond pulses being made available will open the door to attosecond X-ray diffraction, offering the ability to track the motion of electrons in solids with picometre-attosecond space–time resolution for the first time. Capturing the temporal evolution of the spatial probability distribution of electrons will provide access to dynamic processes of matter at the most fundamental level. Moreover, access to transient electron density distributions will provide direct insight into highly sophisticated motions in complex systems, previously inaccessible to time-resolved interrogation.

Parallel to the current exciting progress towards OPCPA-based waveform synthesisers utilising Ti:Sa [79] or Yb:YAG [45] laser technology, recent development in 4 μm and even 7 μm few-cycle laser sources holds promise for yet another revolution in generation of sub-cycle light transients in the near future [80–82].

Acknowledgements

This paper is dedicated to Prof. Ferenc Krausz on the occasion of the 15th anniversary of the first measurement of XUV attosecond pulses. I would like to thank him for sharing with me his thoughtful insights in the field of few-cycle lasers and for the many discussions during the past eight years. I would also like to acknowledge the senior scientist mentioned in the introduction, Prof. Matthias Kling, for his encouragements at the beginning of my PhD.

Disclosure statement

No potential conflict of interest was reported by the authors.

Notes on contributor

Hanieh Fattahi studied Applied physics at Sharif University of Technology in Tehran and received her PhD in Physics at Ludwig Maximilians university of Munich. Since then, she has been a researcher at the Laboratory for Attosecond Physics at the Max Planck Institute of Quantum Optics. Her research centers on Synthesis of intense controlled waveforms of laser light, and Design and development of thin-disk lasers and optical parametric amplifiers. She is the fellow of Max Planck center for Extreme and Quantum Photonics in Ottawa and co-coordinator of the 'International Max-Planck Research School of Advanced Photon Science' (IMPRS-APS). She enjoys Swimming, running, hiking, wine tasting, watching action and Sci-Fi movies, and socialising.

References

[1] D.E. Spence, P.N. Kean, and W. Sibbett, *60-fsec pulse generation from a self-mode-locked Ti:sapphire laser*, Opt. Lett. 16 (1991), pp. 42–44.

[2] T.W. Haensch, *A proposed sub-femtosecond pulse synthesizer using separate phase-locked laser oscillators*, Opt. Commun. 80 (1990), pp. 71–75.

[3] T. Brabec and F. Krausz, *Intense few-cycle laser fields: Frontiers of nonlinear optics*, Rev. Mod. Phys. 72 (2000), pp. 545–591.

[4] D. Gabor, *Theory of communication. Part 1: The analysis of information*, J. Inst. Electr. Eng. – Part III Radio Commun. Eng. 93 (1946), pp. 429–441.

[5] R.W. Boyd, *Nonlinear Optics*, Elsevier, Amsterdam, 2008.

[6] S. Mann and S. Haykin, *The chirplet transform: A generalization of Gabor's logon transform*, Vis. Interface 91 (1991), pp. 205–212.

[7] A.W. Lohmann, D. Mendlovic, and Z. Zalevsky, *Fractional Hilbert transform*, Opt. Lett. 21 (1996), pp. 281–283.

[8] A. Venkitaraman and C.S. Seelamantula, *Fractional Hilbert transform extensions and associated analytic signal construction*, Signal Process. 94 (2014), pp. 359–372.

[9] T. Tsurumi, *Propagation of few- to sub-cycle pulse in dispersive media*, J. Phys. Soc. Japan 75 (2006), pp. 0240021–02400210.

[10] X. Cai, J. Zhao, Q. Lin, J. Luo, and Y. Yang, *Propagation of intrinsic chirped sub-cycle and single-cycle pulses in a silica fiber*, Opt. Commun. 366 (2016), pp. 221–228.

[11] Q. Lin, J. Zheng, and W. Becker, *Subcycle pulsed focused vector beams*, Phys. Rev. Lett. 97 (2006), pp. 2539021–2539024.

[12] P. Corkum, N. Burnett, and F. Brunel, *Above-threshold ionization in the long-wavelength limit*, Phys. Rev. Lett. 62 (1989), pp. 1259–1262.

[13] T.H. Maiman, *Stimulated optical radiation in ruby*, Nature 187 (1960), pp. 493–494.

[14] P. Franken, A. Hill, C. Peters, and G. Weinreich, *Generation of optical harmonics*, Phys. Rev. Lett. 7 (1961), pp. 118–119.

[15] J. Armstrong, N. Bloembergen, J. Ducuing, and P. Pershan, *Interactions between light waves in a nonlinear dielectric*, Phys. Rev. 127 (1962), pp. 1918–1939.

[16] J.A. Valdmanis, R.L. Fork, and J.P. Gordon, *Generation of optical pulses as short as 27 femtoseconds directly from a laser balancing self-phase modulation, group-velocity dispersion, saturable absorption, and saturable gain*, Opt. Lett. 10 (1985), pp. 131–133.

[17] R.L. Fork and C.H. Brito, *Cruz, P. C. Becker, and C. V. Shank, Compression of optical pulses to six femtoseconds by using cubic phase compensation*, Opt. Lett. 12 (1987), pp. 483–485.

[18] W.H. Knox, M.C. Downer, R.L. Fork, and C.V. Shank, *Amplified femtosecond optical pulses and continuum generation at 5-kHz repetition rate*, Opt. Lett. 9 (1984), pp. 552–554.

[19] C. Rolland and P. Corkum, *Amplification of 70 fs pulses in a high repetition rate XeCl pumped dye laser amplifier*, Opt. Commun. 59 (1986), pp. 64–68.

[20] P.F. Moulton, *Spectroscopic and laser characteristics of Ti:Al_2O_3*, J. Opt. Soc. Am. B 3 (1986), pp. 125–133.

[21] R. Szipöcs, C. Spielmann, F. Krausz, and K. Ferencz, *Chirped multilayer coatings for broadband dispersion control in femtosecond lasers*, Opt. Lett. 19 (1994), pp. 201–203.

[22] A. Stingl, R. Szipöcs, M. Lenzner, C. Spielmann, and F. Krausz, *Sub-10-fs mirror-dispersion-controlled Ti:sapphire laser*, Opt. Lett. 20 (1995), pp. 602–604.

[23] A. Kasper and K.J. Witte, *10-fs pulse generation from a unidirectional Kerr-lens mode-locked Ti:sapphire ring laser*, Opt. Lett. 21 (1996), pp. 360–362.

[24] C. Cook, *Pulse compression-key to more efficient radar transmission*, Proc. IRE 48 (1960), pp. 310–316.

[25] D. Strickland and G. Mourou, *Compression of amplified chirped optical pulses*, Opt. Commun. 55 (1985), pp. 447–449.

[26] L. Xu, T.W. Hänsch, C. Spielmann, A. Poppe, T. Brabec, and F. Krausz, *Route to phase control of ultrashort light pulses*, Opt. Lett. 21 (1996), pp. 2008–2010.

[27] F. Krausz and M. Ivanov, *Attosecond physics*, Rev. Mod. Phys. 81 (2009), pp. 163–234.

[28] A.L. Cavalieri, E. Goulielmakis, B. Horvath, W. Helml, M. Schultze, M. Fieß, V. Pervak, L. Veisz, V.S. Yakovlev, M. Uiberacker, A. Apolonski, F. Krausz, and R. Kienberger, *Intense 1.5-cycle near infrared laser waveforms and their use for the generation of ultra-broadband soft-x-ray harmonic continua*, New J. Phys. 9 (2007), pp. 2421–29.

[29] A.M. Weiner, *Femtosecond pulse shaping using spatial light modulators*, Rev. Sci. Instrum. 71 (2000), p. 1929.

[30] S. Bohman, A. Suda, T. Kanai, S. Yamaguchi, and K. Midorikawa, *Generation of 5.0 fs, 5.0 mJ pulses at 1kHz using hollow-fiber pulse compression*, Opt. Lett. 35 (2010), pp. 1887–1889.

[31] W. Schweinberger, A. Sommer, E. Bothschafter, J. Li, F. Krausz, R. Kienberger, and M. Schultze, *Waveform-controlled near-single-cycle milli-joule laser pulses generate sub-10 nm extreme ultraviolet continua*, Opt. Lett. 37 (2012), pp. 3573–3575.

[32] A. Wirth, M.T. Hassan, I. Grguras, J. Gagnon, A. Moulet, T.T. Luu, S. Pabst, R. Santra, Z.A. Alahmed, A.M. Azzeer, V.S. Yakovlev, V. Pervak, F. Krausz, and E. Goulielmakis,

Synthesized light transients, Science 334 (2011), pp. 195–200.

[33] M.T. Hassan, T.T. Luu, A. Moulet, O. Raskazovskaya, P. Zhokhov, M. Garg, N. Karpowicz, A.M. Zheltikov, V. Pervak, F. Krausz, and E. Goulielmakis, *Optical attosecond pulses and tracking the nonlinear response of bound electrons*, Nature 530 (2016), pp. 66–70.

[34] T.T. Luu, M. Garg, S.Y. Kruchinin, A. Moulet, M.T. Hassan, and E. Goulielmakis, *Extreme ultraviolet high-harmonic spectroscopy of solids*, Nature 521 (2015), pp. 498–502.

[35] A. Wirth, R. Santra, and E. Goulielmakis, *Real time tracing of valence-shell electronic coherences with attosecond transient absorption spectroscopy*, Chem. Phys. 414 (2013), pp. 149–159.

[36] M.T. Hassan, A. Wirth, I. Grguraš, A. Moulet, T.T. Luu, J. Gagnon, V. Pervak, and E. Goulielmakis, *Invited article: attosecond photonics: synthesis and control of light transients*, Rev. Sci. Instrum. 83 (2012), pp. 1113011–1113019.

[37] A. Dubietis, G. Jonušauskas, and A. Piskarskas, *Powerful femtosecond pulse generation by chirped and stretched pulse parametric amplification in BBO crystal*, Opt. Commun. 88 (1992), pp. 437–440.

[38] D. Herrmann, L. Veisz, R. Tautz, F. Tavella, K. Schmid, V. Pervak, and F. Krausz, *Generation of sub-three-cycle, 16 TW light pulses by using noncollinear optical parametric chirped-pulse amplification*, Opt. Lett. 34 (2009), pp. 2459–2461.

[39] O.V. Chekhlov, J.L. Collier, I.N. Ross, P.K. Bates, M. Notley, C. Hernandez-Gomez, W. Shaikh, C.N. Danson, D. Neely, P. Matousek, S. Hancock, and L. Cardoso, *35 J broadband femtosecond optical parametric chirped pulse amplification system*, Opt. Lett. 31 (2006), pp. 3665–3667.

[40] S. Adachi, N. Ishii, T. Kanai, A. Kosuge, J. Itatani, Y. Kobayashi, D. Yoshitomi, K. Torizuka, and S. Watanabe, *5-fs, multi-mJ, CEP-locked parametric chirped-pulse amplifier pumped by a 450-nm source at 1 kHz*, Opt. Express 16 (2008), pp. 14341–14352.

[41] H. Fattahi, C. Skrobol, M. Ueffing, Y. Deng, A. Schwarz, Y. Kida, V. Pervak, T. Metzger, Z. Major, and F. Krausz, *High efficiency, multi-mJ, sub 10 fs, optical parametric amplifier at 3 kHz – OSA Technical Digest (online)*, in *Science & Innovations*, Optical Society of America, San Jose, 2012, pp. CTh1N.6.

[42] F. Röser, T. Eidam, J. Rothhardt, O. Schmidt, D.N. Schimpf, J. Limpert, and A. Tünnermann, *Millijoule pulse energy high repetition rate femtosecond fiber chirped-pulse amplification system*, Opt. Lett. 32 (2007), pp. 3495–3497.

[43] P. Russbueldt, T. Mans, G. Rotarius, J. Weitenberg, H.D. Hoffmann, and R. Poprawe, *400W Yb:YAG Innoslab fs-Amplifier*, Opt. Express 17 (2009), pp. 12230–12245.

[44] L.E. Zapata, H. Lin, A.-L. Calendron, H. Cankaya, M. Hemmer, F. Reichert, W.R. Huang, E. Granados, K.-H. Hong, and F.X. Kärtner, *Cryogenic Yb:YAG composite-thin-disk for high energy and average power amplifiers*, Opt. Lett. 40 (2015), pp. 2610–2613.

[45] H. Fattahi, H.G. Barros, M. Gorjan, T. Nubbemeyer, B. Alsaif, C.Y. Teisset, M. Schultze, S. Prinz, M. Haefner, M. Ueffing, A. Alismail, L. Vámos, A. Schwarz, O. Pronin, J. Brons, X.T. Geng, G. Arisholm, M. Ciappina, V.S. Yakovlev, D.-E. Kim, A.M. Azzeer, N. Karpowicz, D. Sutter, Z. Major, T. Metzger, and F. Krausz, *Third-generation femtosecond technology*, Optica 1 (2014), pp. 45–63.

[46] O.H. Heckl, J. Kleinbauer, D. Bauer, S. Weiler, T. Metzger, D.H. Sutter, *Ultrafast Thin-Disk Lasers*, in *Ultrashort Pulse Laser Technology Volume 195 of the series Springer Series in Optical Sciences*, Springer International Publishing, New York, 2016, pp. 93–115. http://link.springer.com/chapter/10.1007/978-3-319-17659-8_5

[47] H. Fattahi, *Third-generation Femtosecond Technology*, Springer theses, Springer International Publishing, Cham, 2015.

[48] R. Danielius, A. Piskarskas, A. Stabinis, G.P. Banfi, P. Di Trapani, and R. Righini, *Traveling-wave parametric generation of widely tunable, highly coherent femtosecond light pulses*, J. Opt. Soc. Am. B 10 (1993), pp. 2222–2232.

[49] G.M. Gale, M. Cavallari, and F. Hache, *Femtosecond visible optical parametric oscillator*, J. Opt. Soc. Am. B 15 (1998), pp. 702–714.

[50] Y. Deng, A. Schwarz, H. Fattahi, M. Ueffing, X. Gu, M. Ossiander, T. Metzger, V. Pervak, H. Ishizuki, T. Taira, T. Kobayashi, G. Marcus, F. Krausz, R. Kienberger, and N. Karpowicz, *Carrier-envelope-phase-stable, 1.2 mJ, 1.5 cycle laser pulses at 2.1 μm*, Opt. Lett. 37 (2012), pp. 4973–4975.

[51] B.E. Schmidt, N. Thiré, M. Boivin, A. Laramée, F. Poitras, G. Lebrun, T. Ozaki, H. Ibrahim, and F. Légaré, *Frequency domain optical parametric amplification*, Nat. Commun. 5 (2014), pp. 36431–36438.

[52] M. Lenzner, J. Krüger, S. Sartania, Z. Cheng, C. Spielmann, G. Mourou, W. Kautek, and F. Krausz, *Femtosecond optical breakdown in dielectrics*, Phys. Rev. Lett. 80 (1998), pp. 4076–4079.

[53] H. Fattahi, A. Alismail, H. Wang, J. Brons, O. Pronin, T. Buberl, L. Vámos, G. Arisholm, A.M. Azzeer, and F. Krausz, *High-power, 1-ps, all-Yb:YAG thin-disk regenerative amplifier*, Opt. Lett. 41 (2016), pp. 1126–1129.

[54] H.-J. Otto, F. Stutzki, N. Modsching, C. Jauregui, J. Limpert, and A. Tünnermann, *2 kW average power from a pulsed Yb-doped rod-type fiber amplifier*, Opt. Lett. 39 (2014), pp. 6446–6449.

[55] M. Kienel, A. Klenke, T. Eidam, S. Hädrich, J. Limpert, and A. Tünnermann, *Energy scaling of femtosecond amplifiers using actively controlled divided-pulse amplification*, Opt. Lett. 39 (2014), pp. 1049–1052.

[56] P. Russbueldt, T. Mans, J. Weitenberg, H.D. Hoffmann, and R. Poprawe, *Compact diode-pumped 1. 1 kW Yb: YAG Innoslab femtosecond amplifier*, Opt. Lett. 35 (2010), pp. 4169–4171.

[57] T. Nubbemeyer, M. Gorjan, A. Alismail, M. Ueffing, H.G. Barros, T. Metzger, D. Sutter, Z. Major, and F. Krausz, *High Average Power kW-scale Yb:YAG Thin-disk Regenerative Amplifier*, *European Conference on Lasers and Electro-Optics and the European Quantum Electronics Conference*, Optical Society of America, Munich, 2015, .

[58] H. Fattahi, H. Wang, A. Alismail and F. F. Krausz, *Towards high-power, multi-TW light transients*,

Conference on Lasers Electro-Optics, OSA, Washington, DC, 2016, pp. SM1M.6.

[59] H. Fattahi, C.Y. Teisset, O. Pronin, A. Sugita, R. Graf, V. Pervak, X. Gu, T. Metzger, Z. Major, F. Krausz, and A. Apolonski, *Pump-seed synchronization for MHz repetition rate, high-power optical parametric chirped pulse amplification*, Opt. Express 20 (2012), pp. 9833–9840.

[60] A. Schwarz, M. Ueffing, Y. Deng, X. Gu, H. Fattahi, T. Metzger, M. Ossiander, F. Krausz, and R. Kienberger, *Active stabilization for optically synchronized optical parametric chirped pulse amplification*, Opt. Express 20 (2012), pp. 5557–5565.

[61] T. Buberl, A. Alismail, H. Wang, N. Karpowicz, and H. Fattahi, *Self-compressed, spectral broadening of a Yb:YAG thin-disk amplifier*, Opt. Express 24 (2016), pp. 10286–10294.

[62] T. Amotchkina, H. Fattahi, Y.A. Pervak, M. Trubetskov, and V. Pervak, *Broadband beamsplitter for high intensity laser applications in the infra-red spectral range*, Opt. Express 24 (2016), pp. 16752–16759.

[63] M. Hentschel, R. Kienberger, C. Spielmann, G.A. Reider, N. Milosevic, T. Brabec, P. Corkum, U. Heinzmann, M. Drescher, and F. Krausz, *Attosecond metrology*, Nature 414 (2001), pp. 509–513.

[64] S. Keiber, S. Sederberg, A. Schwarz, M. Trubetskov, V. Pervak, F. Krausz, and N. Karpowicz, *Electro-optic sampling of near-infrared waveforms*, Nat. Photonics (2016), pp. 1–5.

[65] C. Manzoni, S.-W. Huang, G. Cirmi, P. Farinello, J. Moses, F.X. Kärtner, and G. Cerullo, *Coherent synthesis of ultra-broadband optical parametric amplifiers*, Opt. Lett. 37 (2012), pp. 1880–1882.

[66] P.B. Corkum and F. Krausz, *Attosecond science*, Nat. Phys. 3 (2007), pp. 381–387.

[67] F. Krausz and M.I. Stockman, *Attosecond metrology: From electron capture to future signal processing*, Nat. Photonics 8 (2014), pp. 205–213.

[68] M. Uiberacker, T. Uphues, M. Schultze, A.J. Verhoef, V. Yakovlev, M.F. Kling, J. Rauschenberger, N.M. Kabachnik, H. Schröder, M. Lezius, K.L. Kompa, H.-G. Muller, M.J.J. Vrakking, S. Hendel, U. Kleineberg, U. Heinzmann, M. Drescher, and F. Krausz, *Attosecond real-time observation of electron tunnelling in atoms*, Nature 446 (2007), pp. 627–632.

[69] E. Goulielmakis, Z.-H. Loh, A. Wirth, R. Santra, N. Rohringer, V.S. Yakovlev, S. Zherebtsov, T. Pfeifer, A.M. Azzeer, M.F. Kling, S.R. Leone, and F. Krausz, *Real-time observation of valence electron motion*, Nature 466 (2010), pp. 739–743.

[70] M. Schultze, M. Fiess, N. Karpowicz, J. Gagnon, M. Korbman, M. Hofstetter, S. Neppl, A.L. Cavalieri, Y. Komninos, T. Mercouris, C.A. Nicolaides, R. Pazourek, S. Nagele, J. Feist, J. Burgdorfer, A.M. Azzeer, R. Ernstorfer, R. Kienberger, U. Kleineberg, E. Goulielmakis, F. Krausz, and V.S. Yakovlev, *Delay in photoemission*, Science (80-.). 328 (2010), pp. 658–1662.

[71] A. Rousse, C. Rischel, and J.-C. Gauthier, *Femtosecond x-ray crystallography*, Rev. Mod. Phys. 73 (2001), pp. 17–31.

[72] J. Amann, W. Berg, V. Blank, F.-J. Decker, Y. Ding, P. Emma, Y. Feng, J. Frisch, D. Fritz, J. Hastings, Z. Huang, J. Krzywinski, R. Lindberg, H. Loos, A. Lutman, H.-D. Nuhn, D. Ratner, J. Rzepiela, D. Shu, Y. Shvyd'ko, S. Spampinati, S. Stoupin, S. Terentyev, E. Trakhtenberg, D. Walz, J. Welch, J. Wu, A. Zholents, and D. Zhu, *Demonstration of self-seeding in a hard-X-ray free-electron laser*, Nat. Photonics 6 (2012), pp. 693–698.

[73] A.H. Zewail, *Four-dimensional electron microscopy*, Science 328 (2010), pp. 187–193.

[74] G. Sciaini and R.J.D. Miller, *Femtosecond electron diffraction: Heralding the era of atomically resolved dynamics*, Reports Prog. Phys. 74 (2011), pp. 0961011–09610136.

[75] T. Ishikawa, S.A. Hayes, S. Keskin, G. Corthey, M. Hada, K. Pichugin, A. Marx, J. Hirscht, K. Shionuma, K. Onda, Y. Okimoto, S.-Y. Koshihara, T. Yamamoto, H. Cui, M. Nomura, Y. Oshima, M. Abdel-Jawad, R. Kato, and R.J.D. Miller, *Direct observation of collective modes coupled to molecular orbitaldriven charge transfer*, Science 350 (2015), pp. 1501–1505.

[76] S. Lahme, C. Kealhofer, F. Krausz, and P. Baum, *Femtosecond single-electron diffraction*, Struct. Dyn. 1 (2014), pp. 0343031–0343039.

[77] D. Shorokhov and A.H. Zewail, *Perspective: 4D ultrafast electron microscopy-evolutions and revolutions*, J. Chem. Phys. 144 (2016), pp. 0809011–08090124.

[78] P. Baum, *Towards ultimate temporal and spatial resolutions with ultrafast single-electron diffraction*, J. Phys. B At. Mol. Opt. Phys. 47 (2014), p. 124005.

[79] O.D. Mucke, S. Fang, G. Cirmi, G.M. Rossi, S.-H. Chia, H. Ye, Y. Yang, R. Mainz, C. Manzoni, P. Farinello, G. Cerullo, and F.X. Kartner, *Toward waveform nonlinear optics using multimillijoule sub-cycle waveform synthesizers*, IEEE J. Sel. Top. Quantum Electron. 21 (2015), pp. 1–12.

[80] D. Sanchez, M. Hemmer, M. Baudisch, S.L. Cousin, K. Zawilski, P. Schunemann, O. Chalus, C. Simon-Boisson, and J. Biegert, *7 μm, ultrafast, sub-millijoule-level mid-infrared optical parametric chirped pulse amplifier pumped at 2 μm*, Optica 3 (2016), pp. 147–150.

[81] A.V. Mitrofanov, A.A. Voronin, D.A. Sidorov-Biryukov, A. Pugžlys, E.A. Stepanov, G. Andriukaitis, T. Flöry, S. Ališauskas, A.B. Fedotov, A. Baltuška, and A.M. Zheltikov, *Mid-infrared laser filaments in the atmosphere*, Sci. Rep. 5 (2015), pp. 83681–83686.

[82] T. Popmintchev, M.-C. Chen, D. Popmintchev, P. Arpin, S. Brown, S. Alisauskas, G. Andriukaitis, T. Balciunas, O.D. Mücke, A. Pugzlys, A. Baltuska, B. Shim, S.E. Schrauth, A. Gaeta, C. Hernández-García, L. Plaja, A.Becker, A. Jaron-Becker, M.M. Murnane, and H.C. Kapteyn, *Bright coherent ultrahigh harmonics in the keV x-ray regime from mid-infrared femtosecond lasers*, Science 336 (2012), pp. 1287–1291.